TILT MATCHING FOR SCALABLE SAMPLING AND FINE-TUNING

Anonymous authors

000

001

003 004

010 011

012

013

014

015

016

017

018

019

021

025

026027028

029

031

032

033

034

037

040

041

042

043

044

046

047

048

051

052

Paper under double-blind review

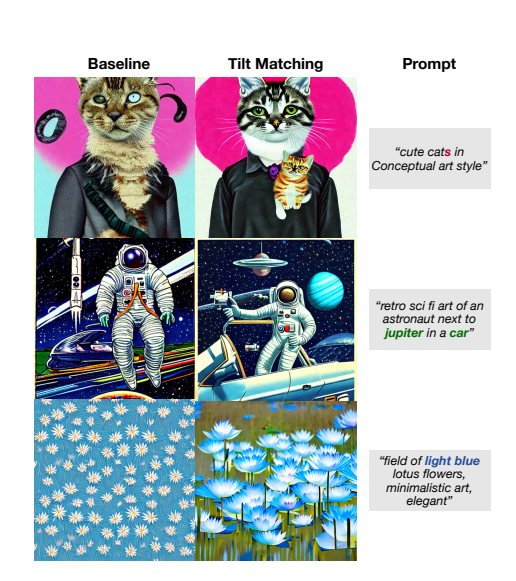
ABSTRACT

We propose a simple, scalable algorithm for using stochastic interpolants to perform sampling from unnormalized densities and for fine-tuning generative models. The approach, Tilt Matching, arises from a dynamical equation relating the velocity field for a flow matching method to the velocity field that would target the same distribution tilted by a reward. As such, the new velocity inherits the regularity of stochastic interpolant transport plans while also being the minimizer of an objective function with strictly lower variance than flow matching itself. The update to the velocity field that emerges from this simple regression problem can be interpreted as the sum of all joint cumulants of the stochastic interpolant and copies of the reward, and to first order is their covariance. We define two versions of the method, Explicit and Implicit Tilt Matching. The algorithms do not require any access to gradients of the reward or backpropagating through trajectories of the flow or diffusion. We empirically verify that the approach is efficient, unbiased, and highly scalable, providing state-of-the-art results on sampling under Lennard-Jones potentials and is competitive on fine-tuning Stable Diffusion, without requiring reward multipliers. It can also be straightforwardly applied to tilting few-step flow map models.

1 Introduction

Generative models built out of dynamical transport like flow and diffusion models are highly scalable tools that serve as building blocks for foundation models across industries (Rombach et al., 2022; Geffner et al., 2025; Watson et al., 2023; Brooks et al., 2024; Zeni et al., 2025). These models work by building a continuous time map connecting a base distribution to a target distribution, realized by solving a differential equation whose coefficients are neural networks.

There is now a vested interest in applying them in settings where there is not *a priori* an abundance of data to learn from to complete a task of interest. These include learning to sample under Boltzmann distributions appearing in molecular dynamics Noé et al. (2019); Herron et al. (2024); Plainer et al. (2025) and statistical physics Albergo et al. (2019); Gabrié et al. (2022); Kanwar et al. (2020); Nicoli et al. (2021), as well as fine-tuning an existing gen-



Gabrié et al. (2022); Kanwar et al. (2020); Nicoli et al. (2021), as well as fine-tuning an existing generative model so as to produce samples that align with user requests.

Figure 1: Example improvements to Stable Diffusion 1.5 using Tilt Matching and ImageReward.

Both of these problems can be framed as *tilting* some existing distribution toward a new target. For Boltzmann sampling, this means adapting the energy function defining the theory; for fine-tuning, this means adapting the base generative model to score highly against a reward r(x). Our aims in this paper are precisely centered around this picture. Given access to samples from a distribution with density $\rho_1(x): \mathbb{R}^d \to \mathbb{R}$, we want to learn to sample the tilted distribution $\rho_{1,a} \propto \rho_1 e^{ar(x)}$, where

r(x) is a scalar function which defines the **tilt** and a is an annealing parameter that characterizes the extent of the tilt. This initial distribution $\rho_1=\rho_{1,a=0}$ could be given by an existing generative model, as in the case of fine-tuning, or it may be a reference distribution that is easy to sample with conventional techniques when performing sampling. We will ultimately be interested in $\rho_{t,a=1}$, i.e. the density fully tilted toward the reward.

While diffusions (Song et al., 2020; Ho et al., 2020), flow-based models (Lipman et al., 2022; Albergo & Vanden-Eijnden, 2022; Liu et al., 2022) work well when data is available, regression objectives for the data-less contexts we focus on here are still not available, or come with caveats. In what follows, we briefly summarize the highly scalable generative models. Then, we will motivate a practical *modification* to these approaches so that they maintain many of their appealing optimization qualities while making them applicable to fine-tuning and sampling. To this end, we specify our **main contributions:**

- We derive an evolution equation for stochastic interpolant velocity fields under reward tilts that has a fundamental connection to the higher order moments between the interpolant and the reward.
- We show how the above fact allows us to construct *Tilt Matching*, a family of simple iterative regression loss functions for the tilted velocity field that do not rely on backpropagating through generated trajectories, do not require spatial gradients of the reward, can avoid likelihood computations during training, and whose variances are strictly less than that of flow matching itself and can be further systematically improved with control variates.
- We instantiate two versions of the objective, Explicit Tilt Matching and Implicit Tilt Matching; the latter completely removes discretization errors from iteratively updating the tilt.
- We show how the method can be applied to both sampling distributions known up to normalizing constant and to fine-tuning existing generative models, where we achieve state-of-the-art performance on sampling Lennard-Jones potentials, and can improve perceptual scores of Stable Diffusion 1.5 with straightforward application of the algorithm.

2 RELATED WORK

Neural Samplers Employing transport in Monte Carlo sampling algorithms has been an active research topic beginning with the work of Marzouk et al. (2016), and made parametric with neural networks in (Noé et al., 2019; Albergo et al., 2019), using coupling-based normalizing flows (Rezende & Mohamed, 2015; Dinh et al., 2017). Recent works have sought to perform this sampling with continuous time flow and diffusion models. These "neural samplers" take on various forms. Some approach the problem from an optimal control perspective (Zhang & Chen, 2022; Tzen & Raginsky, 2019; Havens et al., 2025) involving backpropagating through stochastic trajectories. Others interface with annealed importance sampling Neal (1993) and attempt to learn drift coefficients along a geometric annealing path either through trajectories (Vargas et al., 2024) or Physics Informed Neural Network (PINN) objectives (Máté & Fleuret, 2023; Tian et al., 2024; Albergo & Vanden-Eijnden, 2024; Holderrieth et al., 2025). The trajectory based losses can become unstable if the number of steps taken in solving the SDE is not sufficiently small, and while the PINN based losses avoid this, they can sometimes involve unstable or expensive terms based off of derivatives of neural networks in the loss function. Other works like (Vargas et al., 2023) also try to learn to sample along the time-dependent density of a diffusion process, but their formulation requires backpropagating through trajectories. Our proposed approach inherits the potential efficiency of coupling based flows because all of it can be defined with the any step flow map (Boffi et al., 2024; 2025; Sabour et al., 2025); does not rely on backpropagating through trajectories; does not require computation of likelihoods; and does not require enforcing a PINN loss with gradients of neural networks in it.

Fine-tuning flows and diffusions Modifying the drift of the generative process is the predominant strategy for fine-tuning dynamical transport models. Existing work follows two high-level approaches: 1) reward-maximizing methods that directly optimize the quality of generated samples, such as D-Flow Ben-Hamu et al. (2024) and DRaFT Clark et al. (2024), and 2) distribution matching techniques that align the model with a reward-tilted distribution to prevent overfitting, seen in DEFT (Denker et al., 2024), adjoint matching (Domingo-Enrich et al., 2025), GFlowNet approaches

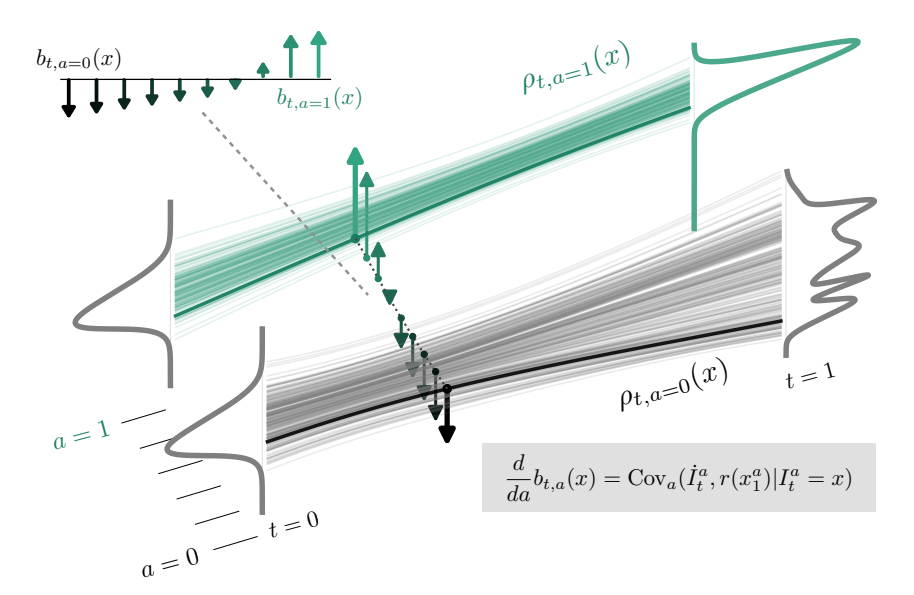


Figure 2: Schematic overview of the proposed method. When a stochastic interpolant is used to learn a generative model $b_{t,a=0}$ that samples $\rho_{t,a=0}$ and in particular $\rho_{1,a=0}$ (gray curve), then the evolution of that velocity field in a in order to sample $\rho_{1,a>0}=\frac{1}{Z}\rho_{1,0}e^{ar(x)}$, where r is a reward function, has closed form given by the covariance of the dynamics of the interpolant at (t,a) and the reward. The velocity field, denoted as up or down arrows showing direction of motion in x, changes from negative to positive in the above toy example.

(Zhang et al., 2024; Liu et al., 2025), and approaches adapted from DPO Wallace et al. (2024). Nevertheless, these algorithms frequently suffer from major disadvantages, including the need to differentiate through trajectories Denker et al. (2024); Ben-Hamu et al. (2024); Clark et al. (2024) or the requirement of a differentiable reward function (Ben-Hamu et al., 2024; Clark et al., 2024; Zhang et al., 2024; Liu et al., 2025; Domingo-Enrich et al., 2025), while some are only approximate Wallace et al. (2024). The proposed tilt matching method is free from these limitations.

2.1 DYNAMICAL TRANSPORT, STOCHASTIC INTERPOLANTS, AND FLOW MAPS

Many state-of-the-art generative models that aim to model a data distribution $\rho_1(x)$ learned from samples $\{x_1\}_{i=1}^N$ do so by means of dynamically mapping samples from a reference distribution $x_0 \sim \rho_0$. This mapping is defined by a drift coefficient in a flow Albergo & Vanden-Eijnden (2022); Lipman et al. (2022) or diffusion process Song et al. (2020); Ho et al. (2020), e.g. appearing in the ordinary differential equation (ODE)

$$\dot{x}_t = b_t(x_t), \qquad x_0 \sim \rho_0 \tag{1}$$

where $b_t: [0,1] \times \mathbb{R}^d \to \mathbb{R}^d$ is a vector field that governs the transport such that the solution to equation 1 up to time t produces a sample $x_t \sim \rho_t$. The PDF ρ_t of this process satisfies the continuity equation

$$\partial_t \rho_t + \nabla \cdot (b_t \rho_t) = 0, \qquad \rho_{t=0} = \rho_0.$$
 (2)

In generative modeling, our aims are to learn b_t over neural networks such that the marginal law arising from (1) satisfy (2). A highly scalable, unifying perspective for dynamical transport models is that of stochastic interpolants Albergo & Vanden-Eijnden (2022); Albergo et al. (2023). A stochastic interpolant $I_t(x_0, x_1) : [0, 1] \times \mathbb{R}^d \times \mathbb{R}^d \to \mathbb{R}^d$ defined as

$$I_t := \alpha_t x_0 + \beta_t x_1 \qquad x_0, x_1 \sim \rho(x_0, x_1),$$
 (3)

where α_t, β_t are functions of time satisfying $\alpha_0 = \beta_1 = 1$ and $\alpha_1 = \beta_0 = 0$, is a stochastic process such that Law $(I_t) = \rho_t$. Importantly, the velocity field associated to this ρ_t which solves equation 2 has a closed form which is given by $b_t(x) = \mathbb{E}[\dot{I}_t|I_t = x]$, where the expectation is taken over the

coupling $(x_0, x_1) \sim \rho(x_0, x_1)$ conditional on $I_t = x$. Plugging this expression into a regression loss function to learn b_t over neural networks gives, by tower property of the conditional expectation,

$$b_t = \arg\min_{\hat{b}_t} \int_0^1 \mathbb{E} \left| \hat{b}_t(I_t) - \dot{I}_t \right|^2 dt. \tag{4}$$

This procedure is the backbone of various large-scale generative models across various domains such as image and video generation Esser et al. (2024) and protein design Geffner et al. (2025). The main question to keep in mind going forward is: how is the solution b_t of one transport problem related to the solution of another?

2.2 FINE TUNING AND SAMPLING AS TILTING

One might ask how this b_t could be modified such that it solves the transport not for ρ_1 , but rather the tilted distribution $\rho_{1,a}$ which defines our fine-tuning or sampling problem. That is, how are the velocity fields $b_{t,a=0}$ and $b_{t,a>0}$ related, and is there a learning paradigm that would allow us to estimate $b_{t,a}$ when initially given access only to the ground truth velocity field $b_{t,0}$ for the original generative model? This would allow us to ultimately evolve $b_{t,a}$ all the way to $b_{t,1}$, which would be the velocity field that can be used to directly sample the tilted distribution. We now introduce our method focused on this evolution, which we call **Tilt Matching Models** (**TMMs**), a scalable procedure for adapting velocity fields under tilting.

3 DERIVING TILT MATCHING

To approach this question, consider modifying (3) so that it instead uses samples $x_1^a \sim \rho_{1,a}$

$$I_t^a := \alpha_t x_0 + \beta_t x_1^a \tag{5}$$

i.e. $\operatorname{Law}(I^a_t) = \rho_{t,a}$. Learning the velocity directly from this interpolant would be convenient, but we do not have samples a priori under $\rho_{t,a>0}$ to construct it, so this object is not immediately useful. However, it is possible to define $b_{t,a}$ in terms of the original interpolant, which we do have access to, combined with weights via:

$$b_{t,a}(x) = \frac{\mathbb{E}[\dot{I}_t^0 e^{ar(x_1)} | I_t^0 = x]}{\mathbb{E}[e^{ar(x_1)} | I_t^0 = x]}.$$
 (6)

This relation is proven in the appendix, and it also straightforwardly holds for a shift of arbitrary size h from a to a + h:

$$b_{t,a+h}(x) = \frac{\mathbb{E}[\dot{I}_t^a e^{hr(x_1)} | I_t^a = x]}{\mathbb{E}[e^{hr(x_1)} | I_t^a = x]}.$$
 (7)

If h is large, then the variance of this expression may make any computational realizations of it impractical. Instead, by taking the derivative of (7) with respect to a, we can ask how $b_{t,a}$ should evolve to anneal it toward our target velocity field. The following proposition shows that the *evolution* of the velocity field $b_{t,a}(x)$ associated to equation 5 with respect to a has a closed form defined solely in terms of known or learnable quantities:

Proposition 1. (Covariance ODE.) Let $I_t^a = \alpha_t x_0 + \beta_t x_1^a$ be the interpolant constructed from samples $x_1^a \sim \rho_{1,a}(x)$. Then the augmented drift $b_{t,a}(x)$ satisfies

$$\frac{\partial b_{t,a}(x)}{\partial a} = \mathbb{E}[\dot{I}_t^a r(x_1^a) | I_t^a = x] - b_{t,a}(x) \, \mathbb{E}[r(x_1^a) | I_t^a = x], \qquad b_{t,a=0}(x) = b_t(x) \tag{8}$$

where the expectation is taken over the law of I_t^a conditional on $I_t^a = x$. The right-hand side of this equation is the conditional covariance $\operatorname{Cov}_a(\dot{I}_t^a, r(x_1^a) | I_t^a = x)$.

Proposition 1 is proven in Appendix A. The above relation can be interpreted as a dynamical formulation of the Esscher transform (Esscher, 1932) arising from (7). The Esscher transform characterizes how expectations evolve under exponential tiltings. Here, applied to stochastic interpolant velocity fields, tilting by $e^{hr(x)}$ induces a flow on $b_{t,a}$ whose infinitesimal generator is the conditional covariance between the interpolant and the reward. Importantly, this evolution of $b_{t,a}$ with respect to a only depends on the current $b_{t,a}(x)$, the modified interpolant equation 5, and the reward.

 $b_{t,a+h}(x) = b_{t,a}(x) + h \frac{\partial b_{t,a}(x)}{\partial a} + \mathcal{O}(h^2)$

219 220 221

First order expansion. Because we can use the current $b_{t,a}(x)$ (or its flow map equivalent) to produce samples x_1^a , this suggests that the corrections to $b_{t,a=0}$ that need to be learned to sample the true tilted density can be learned in an iterative fashion by discretizing equation 8. That is, for $0 < h \ll 1$, we can write an **explicit Euler discretization** as

 $= b_{t,a}(x) + h \Big(\mathbb{E} \Big[\dot{I}_t^a \, r(x_1^a) \, \Big| \, I_t^a = x \Big] - b_{t,a}(x) \, \mathbb{E} [r(x_1^a) \, | \, I_t^a = x] \, \Big) + \mathcal{O}(h^2).$

This perspective highlights TM as an iterative, covariance-guided procedure: starting from $b_{t,0}$,

one can generate successive updates $b_{t,h}, b_{t,2h}, \ldots, b_{t,1}$ that gradually transform the velocity field

toward the fully tilted distribution. As $h \to 0$, this discretization recovers the continuous evolution

in equation 8, ensuring convergence to the desired $b_{t,1}$. To formalize this, we introduce the **residual**

222

224

225

230

231

233

234 235

236

237 238 239

240 241

242 243

244 245

246 247 248

249 250 251

253 254 255

256

257

> 264 265 266

267

268

269

262

263

 $T_{t,a,h}^{\mathrm{ETM}} := b_{t,a}(I_t^a) + \underbrace{h\Big(\dot{I}_t^a\,r(x_1^a) - b_{t,a}(I_t^a)\,r(x_1^a)\Big)}_{\text{residual}}.$ 232

The following proposition shows that $b_{t,a+h}$ can be efficiently regressed and is first-order accurate using what we call **Explicit Tilt Matching** (ETM):

Proposition 2. (Explicit Tilt Matching.) Assume $a \mapsto b_{t,a}(x)$ is C^1 with $\partial_a b_{t,a}$ given by (8), and let h > 0. Then, the unique minimizer of the regression objective

$$\mathcal{L}_{a\to a+h}^{\text{ETM}}(\hat{b}) := \int_{0}^{1} \mathbb{E} \left\| \hat{b}_{t}(I_{t}^{a}) - T_{t,a,h} \right\|^{2} dt.$$
 (12)

is given by

operator:

$$\hat{b}_{t,a+h}(x) = \mathbb{E}^a[T_{t,a,h} | I_t^a = x]. \tag{13}$$

(9)

(10)

(11)

As such, training $\hat{b}_{t,a+h}$ to optimality on (12) produces a first-order accurate Euler update of the tilted velocity. Iterating for $a_k = kh$ with samples $x_1^{a_k}$ drawn using the current model defines a consistent scheme that converges to $b_{t,1}$ as $h \to 0$ under the above regularity.

This procedure is appealing because it gives a velocity field $b_{t,a=1}$ with favorable regularity conditions since the ultimate transport from $\rho_{t=0,a=1}$ to $\rho_{t=1,a=1}$ follows the interpolant path. This should make $b_{t,a=1}$ well-posed to be estimated with neural networks, as the transport for such paths starting from the Gaussian is geometrically smooth and does not exhibit any teleportation. At the same time, there are two main approximation errors to account for, which we outline next.

Approximation error due to incomplete minimization of the objective. A first source of error arises if the regression problem in (12) is not minimized exactly at each iteration. This means the learned drift $b_{t,a}$ may deviate from the ideal $b_{t,a}$, with errors compounding over successive updates. To mitigate this, we periodically "refresh" the model by performing flow matching either on newly generated samples, on samples stored in a buffer, or on buffered samples further refined with MCMC steps. This guarantees that the drift remains a valid stochastic interpolant, after which tilting can safely continue. Another complementary approach is to introduce importance weights during training, which corrects for residual mismatch between the model distribution and the tilted target. Together, these strategies effectively debias the procedure and prevent incomplete optimization from undermining convergence.

Discretization error in a. A second source of error comes from discretizing the Covariance ODE in the annealing parameter a. Since (8) defines a continuous evolution, replacing it with discrete steps introduces a bias. In practice, this issue is negligible: we typically choose h to be very small, so the resulting discretization bias can be almost completely eliminated. Moreover, the step size can be adapted dynamically using diagnostic quantities such as effective sample size (ESS) or changes in the estimated drift, which ensures the updates remain close to the continuous trajectory. However, computing diagnostics like the ESS can be computationally expensive, as it often requires calculating the divergence of the learned vector field. This motivates an alternative approach that eliminates discretization error by construction, rather than managing it with this adaptive scheme.

3.2 IMPLICIT TILT MATCHING

Higher order expansions. The explicit scheme defined by (12) arises by discretizing the evolution of $b_{t,a}$ given in (8) with a forward Euler step. While convenient, such updates inherit a discretization bias, which, even if small, might compound over successive steps in a. A natural extension is to consider taking higher-order Taylor expansions. Extending (9) to all orders gives

$$b_{t,a+h}(x) = b_{t,a}(x) + \sum_{n>0} \frac{h^n}{n!} \frac{\partial^n}{\partial a^n} [b_{t,a}(x)].$$
 (14)

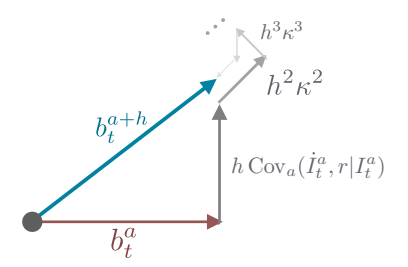


Figure 3: Pictorial additivity of higher order corrections to $b_{t,a+h}$. First order is the covariance, while higher order terms are cumulants κ^n .

This statement on its own is contentless, but the following proposition shows that each term in the expansion has rich meaning:

Proposition 3. (Tilt expansion.) For $b_{t,a} = \mathbb{E}[\dot{I}_t^a | I_t^a = x]$, the n^{th} term $\frac{\partial^n}{\partial a^n}[b_{t,a}(x)]$ in the expansion in (14) is the $(n+1)^{th}$ order joint cumulant of the interpolant and n instances of the reward, $\kappa^n(\dot{I}_t^a, r(x_1^a), \ldots, r(x_1^a))$.

This result is proven in Appendix A and relies on a relation between the Esscher representation of $b_{t,a+h}$ and the moment generating function of the interpolant density. Since the cumulants involve higher order moments of the reward, a Monte Carlo training objective that attempts to match these term by term would be computationally infeasible.

Expanding to all orders. In order to fully eliminate the discretization error, we should consider all higher-order cumulants. Surprisingly, this expression is tractable as we show in the following proposition. If we define the **implicit residual operator** as

$$T_{t,a,h}^{\text{ITM}} := b_{t,a}(I_t^a) + \underbrace{\left(e^{hr(x_1^a)} - 1\right)\left(b_{t,a+h}(x) - \dot{I}_t^a\right)}_{\text{residual}},\tag{15}$$

then we can learn the infinite cumulant expansion by directly matching against it:

Proposition 4. (Implicit Tilt Matching.) Let $b_{t,a+h}$ be defined to all orders as in (14). Then

$$\sum_{n\geq 0} \frac{h^n}{n!} \frac{\partial^n}{\partial a^n} \left[b_{t,a}(x) \right] = \mathbb{E}\left[\left(e^{hr(x_1^a)} - 1 \right) \left(b_{t,a+h}(x) - \dot{I}_t^a \right) | I_t^a = x \right] \tag{16}$$

and $b_{t,a+h}$ is the minimizer of

$$\mathcal{L}_{a\to a+h}^{\mathrm{ITM}}(\hat{b}) := \int_0^1 \mathbb{E} \left\| \hat{b}_t(I_t^a) - T_{t,a,h}^{\mathrm{ITM}} \right\|^2 dt, \tag{17}$$

for any h, where expectation is taken over $(x_0, x_1^a) \sim \rho(x_0, x_1^a)$ conditional on $I_t^a = x$.

This result removes the discretization error inherent to ETM and shows that all orders of the correction to the interpolant velocity field are directly learnable. Enforcing (16) is equivalent to enforcing that the residual update to $b_{t,a+h}$ is exact to all orders. We call this condition **implicit** tilt matching because the residual term that we add to $b_{t,a}$ depends on $b_{t,a+h}$ itself, leading to this fixed-point method.

The expression on the right-hand side of (16) may seem opaque, but it can be motivated with a simple derivation. Starting from the expression for the velocity $b_{t,a+h}$ in (7), we can multiply by the

conditional expectation of the weight $\mathbb{E}[e^{hr(x)}|I_t^a=x]$ and rearrange terms to obtain the optimality condition for (17) in terms of $b_{t,a+h}$

$$\mathbb{E}\Big[e^{hr(x_1^a)}\left(b_{t,a+h}(x) - \dot{I}_t^a\right) \,\Big|\, I_t^a = x\Big] = 0.$$
(18)

Notice that if we take h to be small, replace $e^{hr(x_1^a)} \approx 1 + hr(x_1^a)$ and replace one of the $b_{t,a+h}$ with $b_{t,a}$, then we recover the optimality condition of ETM. Thus we can view Implicit Tilt Matching as a generalization of the discretized procedure in (9) since its linearization recovers the ETM covariance update as specified by (9).

Variance reduction via control variates. We can further introduce a control variate $c(x) : \mathbb{R}^d \to \mathbb{R}$ into (18) to obtain a generalized optimality condition

$$\mathbb{E}\Big[c(x)\left(b_{t,a+h}(x) - b_{t,a}(x)\right) + \left(e^{hr(x_1^a)} - c(x)\right)\left(b_{t,a+h}(x) - \dot{I}_t^a\right) \middle| I_t^a = x\Big] = 0,$$
 (19)

where we used the fact that $\mathbb{E}[c(x)\dot{I}_t^a|I_t^a=x]=\mathbb{E}[c(x)b_{t,a}(x)|I_t^a=x]$. The identity (19) holds for any choice of c(x) and therefore suggests a family of valid implicit objectives we could use to find $b_{t,a+h}$. If we enforce (19) via a regression loss, the c-ITM objective would take the general form of

$$\mathcal{L}_{a\to a+h}^{c-\text{ITM}}(\hat{b}) = \int_{0}^{1} \mathbb{E} \left\| c(I_{t}^{a}) \left(\hat{b}_{t}(I_{t}^{a}) - b_{t,a}(I_{t}^{a}) \right) + \left(e^{hr(x_{1}^{a})} - c(I_{t}^{a}) \right) \left(\hat{b}_{t}(I_{t}^{a}) - \dot{I}_{t}^{a} \right) \right\|^{2} dt \quad (20)$$

The role of c(x) is to control the variance of the Monte Carlo estimator of the loss function. Notice that the choice c(x)=1 recovers (17) exactly. Moreover, this choice has the convenient property that for $h\ll 1$, it is close to the optimal control variate since c(x)=1 clearly minimizes the variance conditional on $I_t^a=x$ when h=0. (See the proof of Proposition 5.) More generally, one can optimize c(x) to minimize the variance, yielding adaptive control variates that further stabilize training.

In practice when h is very small, these higher order cumulants are likely negligible, and this process is still driven by the covariance. Nonetheless, it is now robust to any discretization errors, which we will explore experimentally later.

3.3 REWEIGHTING FLOW MATCHING VERSUS TILT MATCHING

In principle, the tilted drift $b_{t,a+h}$ could be obtained by applying flow matching directly to the interpolant I_t^{a+h} with samples $x_1^{a+h} \sim \rho_{1,a+h}$:

$$b_{t,a+h} = \arg\min_{\hat{b}_t} \int_0^1 \mathbb{E}\left[\left\| \hat{b}_t(I_t^{a+h}) - \dot{I}_t^{a+h} \right\|^2 \right] dt.$$
 (21)

Since we do not have samples from $\rho_{t,a+h}$, the expectation in (21) must be expressed in terms of $\rho_{t,a}$, from which we do have samples. Introducing importance weights leads to what we call the reweighted flow matching (WFM) objective:

$$L_{a\to a+h}^{\text{WFM}}(\hat{b}) = \int_{0}^{1} \mathbb{E}\left[e^{hr(x_{1}^{a})} \|\hat{b}_{t}(I_{t}^{a}) - \dot{I}_{t}^{a}\|^{2}\right] dt.$$
 (22)

Notice that this is precisely the c-ITM loss with c(x)=0. Therefore it has the same expected loss as any c-ITM variant. What differs between the different algorithms is how the Monte Carlo estimates of the loss are taken: WFM regresses directly on \dot{I}_t^a , whereas ITM substitutes the dynamics of stochastic interpolant \dot{I}_t^a with its conditional expectation $b_{t,a}(I_t^a)$. As such, ITM enjoys strictly lower variance than the WFM objective, at least for sufficiently small h:

Proposition 5. (Variance control). Let $\mathcal{L}_{a\to a+h}^{\mathrm{WFM}}$ and $\mathcal{L}_{a\to a+h}^{\mathrm{ITM}}$ be the regression losses in (22) and (12). For sufficiently small h, the gradient estimator of WFM has variance at least as large as that of ACM:

$$\operatorname{Var}\left[\nabla \mathcal{L}_{a \to a + h}^{\operatorname{WFM}}\right] \geq \operatorname{Var}\left[\nabla \mathcal{L}_{a \to a + h}^{\operatorname{ITM}}\right].$$
 (23)

This result formalizes that ITM enjoys a variance advantage over WFM because it centers updates on the conditional mean $b_{t,a}(I_t^a)$ rather than the noisy sample \dot{I}_t^a . We find this bound to have a meaningful implication in numerical experiments.

4 NUMERICAL EXPERIMENTS

An algorithm detailing the numerical implementation of ETM or ITM are given in Appendix B. In what follows, we test the proposed algorithms on both sampling Lennard-Jones (LJ) potentials (of 13 and 55 particles) and fine-tuning Stable Diffusion v1.5. For both setups, we build on existing code bases, e.g. from (Akhound-Sadegh et al., 2025) for the LJ experiments and (Domingo-Enrich et al., 2025; Blessing et al., 2025) for the fine-tuning. All network architectures are the same unless otherwise stated.

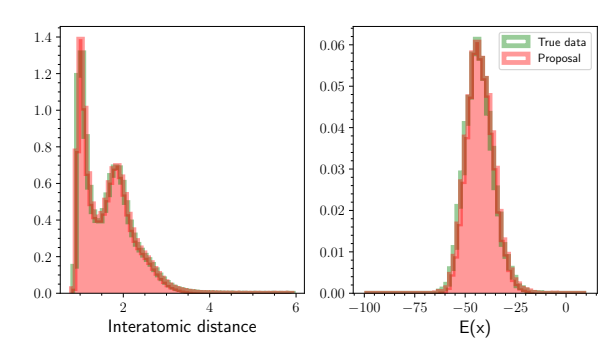


Figure 4: Comparison of LJ13 results using explicit tilt matching vs ground truth molecular dynamics data. **Left:** Histogram of interatomic distances amongst particles in the system. **Right:** Histogram of the energy of 10000 samples of the system. The method shows strong alignment with both measures.

4.1 Sampling Lennard-Jones Potentials

In the context of sampling, the goal is to draw samples from a target density ρ_1 , which is typically the Boltzmann distribution for a given potential energy function $E_1(x)$, such that $\rho_1(x) \propto \exp(-E_1(x))$. For TM, we begin with a simple prior density, $\rho_{1,a=0}$, which corresponds to an initial potential $E_0(x)$, and define an annealing path via linear interpolation:

$$E_a(x) = (1 - a)E_0(x) + aE_1(x). (24)$$

This defines a family of densities $\rho_{1,a}(x) \propto \exp(-E_a(x))$ for $a \in [0,1]$. This path is equivalent to the geometric annealing path described by the reward tilt formulation, where the reward is given by:

$$r(x) = E_0(x) - E_1(x) (25)$$

A common choice for the prior $\rho_{1,a=0}$ is a Gaussian distribution. For molecular systems, a more effective strategy is to define the prior as a high-temperature analogue of the target by setting the initial potential as $E_0(x)=E_1(x)/T_0$, where $T_0\gg 1$ is a high temperature. The resulting prior, $\rho_{1,a=0}\propto \exp(-E_1(x)/T_0)$, has a smoothed energy landscape that facilitates more efficient MCMC sampling. We adopt this temperature annealing approach for our numerical experiments.

We measure the performance of Tilt Mdatching against other methods by computing the effective sample size (ESS), the 2-Wasserstein distances on the energy and interatomic distance between the ground truth and our model outputs. We use the code from (Akhound-Sadegh et al., 2025) to perform the calculation. Note that their code attempts to replicate the Dist W_2 as it appears in (Havens et al., 2025), which is also where the results for DDS and PIS come from, but that code is not available for exact reproduction.

Table 1: Performance comparison on LJ-13 and LJ-55 using the effective sample size, 1D Energy histogram 2-Wasserstein and Distance 2-Wasserstein metrics. Our methods ETM and ITM outperform all previous works across all metrics. Missing — entries indicate the metric is not applicable to that method or not available. We omit the ESS comparison for LJ-55 because it is too computationally intensive for us to compute, and other works do not provide a number to juxtapose with for similar reason.

	LJ-13		LJ-55		
Method	ESS ↑	$E(\cdot) \mathcal{W}_2 \downarrow$	Dist $W_2 \downarrow$	$E(\cdot) \mathcal{W}_2 \downarrow$	Dist $W_2 \downarrow$
DDS (Vargas et al., 2023)	0.101	24.61	1.99	173.09	4.60
PIS (Zhang & Chen, 2022)	0.004	1.93	18.02	228.70	4.79
iDEM (Akhound-Sadegh et al., 2024)	0.231	1.352	0.127	93.53	4.69
Adjoint Sampling (Havens et al., 2025)		2.40	1.67	58.04	4.50
PITA (Akhound-Sadegh et al., 2025)		2.26	0.040	_	_
ETM (Ours)	0.740	0.270	0.012	_	_
ITM (Ours)	0.507	0.879	0.014	29.52	0.054

We highlight a key advantage of ITM is its computational efficiency, as it performs well without requiring an adaptive annealing schedule. This contrasts with our implementation of ETM, where its

strong performance relies on an adaptive schedule guided by the ESS. The ESS calculation, however, requires computing the divergence of the learned vector field, which is a computationally intensive step. The overhead from this calculation made applying our adaptive ETM to larger systems such as LJ-55 impractical, highlighting that ITM is a more scalable and efficient algorithm.

4.2 Fine-tuning Stable Diffusion 1.5

To validate our proposed method, we finetune Stable Diffusion 1.5 (Rombach et al., 2022) using the ImageReward score (Xu et al., 2023) as the objective. Our implementation builds upon the codebase and parameters established in (Domingo-Enrich et al., 2025; Blessing et al., 2025). As our method operates within the stochastic interpolant framework (Albergo et al., 2023), we adopt the necessary transformations to recast the underlying denoising diffusion model, following the procedure detailed in the Appendix of (Domingo-Enrich et al., 2025).

To ensure a comprehensive evaluation and mitigate concerns of overfitting to a single reward metric, we assess performance across three distinct axes: (1) text-to-image consistency, measured by CLIP-Score (Hessel et al., 2021); (2) human aesthetic preference, quantified by HPSv2 (Wu et al., 2023); and (3) sample diversity, evaluated with DreamSim (Fu et al., 2023). We primarily benchmark

Method	ClipScore (\uparrow)	HPSv2 (↑)	DreamSim (†)
Stable Diffusion 1.5 (Base)	0.2771 ± 0.0034	0.2417 ± 0.0032	0.4025 ± 0.0115
Adjoint Matching ($\lambda = 1$)	0.2768 ± 0.0034	0.2426 ± 0.0032	0.4007 ± 0.0114
Adjoint Matching ($\lambda = 10^2$)	0.2798 ± 0.0034	0.2616 ± 0.0030	0.3455 ± 0.0106
ETM $(\lambda = 1)$	0.2801 ± 0.0036	0.2655 ± 0.0029	0.3530 ± 0.0118

Table 2: Finetuning results on Stable Diffusion 1.5. We compare our method against Adjoint Matching (Domingo-Enrich et al., 2025). We report on ClipScore (Hessel et al., 2021), HPSv2 (Wu et al., 2023), and DreamSim (Fu et al., 2023). For all metrics, higher values are better, as indicated by the up-arrow (↑).

against adjoint matching (Domingo-Enrich et al., 2025), the current state-of-the-art for reward fine-tuning, which has demonstrated superior performance over prominent methods like DRaFT (Clark et al., 2024), DPO (Wallace et al., 2024), and ReFL (Xu et al., 2023).

Our results are summarized in Table 2, example images can be found in C. It is standard practice for adjoint matching to employ a reward multiplier, λ , which amplifies the reward signal to steer the learned distribution towards $\rho_1(x)e^{(\lambda\times r(x))}$. A key finding in our experiments is that our method achieves competitive performance against this strong baseline without a need for such a multiplier $(\lambda=1)$ or other hyperparamter tuning. This suggests that our approach provides a direct and stable mechanism for incorporating reward signals into the generation process, likely due to the fact that it does not rely on spatial gradients of the reward for training or generation. Further gains could likely be made by hyperparameter sweeps. We also observed that the implicit version of the tilt matching algorithm can be unstable during fine-tuning, as the magnitude of $\exp(h\times r(x))$ is highly sensitive to the scale of the reward function. In contrast, Euler Tilt Matching with small increments generally trains very stably without much tuning and is therefore recommended for this purpose.

REFERENCES

Tara Akhound-Sadegh, Jarrid Rector-Brooks, Avishek Joey Bose, Sarthak Mittal, Pablo Lemos, Cheng-Hao Liu, Marcin Sendera, Siamak Ravanbakhsh, Gauthier Gidel, Yoshua Bengio, Nikolay Malkin, and Alexander Tong. Iterated denoising energy matching for sampling from boltzmann densities, 2024. URL https://arxiv.org/abs/2402.06121.

Tara Akhound-Sadegh, Jungyoon Lee, Avishek Joey Bose, Valentin De Bortoli, Arnaud Doucet, Michael M. Bronstein, Dominique Beaini, Siamak Ravanbakhsh, Kirill Neklyudov, and Alexander Tong. Progressive inference-time annealing of diffusion models for sampling from boltzmann densities, 2025. URL https://arxiv.org/abs/2506.16471.

Michael S Albergo and Eric Vanden-Eijnden. Building normalizing flows with stochastic interpolants. In *The Eleventh International Conference on Learning Representations*, 2022.

- Michael S. Albergo and Eric Vanden-Eijnden. Nets: A non-equilibrium transport sampler, 2024. URL https://arxiv.org/abs/2410.02711.
 - Michael S Albergo, Nicholas M Boffi, and Eric Vanden-Eijnden. Stochastic interpolants: A unifying framework for flows and diffusions. *arXiv* preprint arXiv:2303.08797, 2023.
 - M.S. Albergo, G. Kanwar, and P.E. Shanahan. Flow-based generative models for markov chain monte carlo in lattice field theory. *Physical Review D*, 100(3), August 2019. ISSN 2470-0029. doi: 10.1103/physrevd.100.034515. URL http://dx.doi.org/10.1103/PhysRevD. 100.034515.
 - Heli Ben-Hamu, Omri Puny, Itai Gat, Brian Karrer, Uriel Singer, and Yaron Lipman. D-flow: Differentiating through flows for controlled generation. In *Forty-first International Conference on Machine Learning*, 2024. URL https://openreview.net/forum?id=SE20BFqj6J.
 - Denis Blessing, Julius Berner, Lorenz Richter, Carles Domingo-Enrich, Yuanqi Du, Arash Vahdat, and Gerhard Neumann. Trust region constrained measure transport in path space for stochastic optimal control and inference, 2025. URL https://arxiv.org/abs/2508.12511.
 - Nicholas M. Boffi, Michael S. Albergo, and Eric Vanden-Eijnden. Flow Map Matching: A unifying framework for consistency models. *arXiv:2406.07507*, June 2024.
 - Nicholas M. Boffi, Michael S. Albergo, and Eric Vanden-Eijnden. How to build a consistency model: Learning flow maps via self-distillation, 2025. URL https://arxiv.org/abs/2505.18825.
 - Tim Brooks, Bill Peebles, Connor Holmes, Will DePue, Yufei Guo, Li Jing, David Schnurr, Joe Taylor, Troy Luhman, Eric Luhman, Clarence Ng, Ricky Wang, and Aditya Ramesh. Video generation models as world simulators. 2024. URL https://openai.com/research/video-generation-models-as-world-simulators.
 - Kevin Clark, Paul Vicol, Kevin Swersky, and David J. Fleet. Directly fine-tuning diffusion models on differentiable rewards. In *The Twelfth International Conference on Learning Representations*, 2024. URL https://openreview.net/forum?id=1vmSEVL19f.
 - Alexander Denker, Francisco Vargas, Shreyas Padhy, Kieran Didi, Simon V Mathis, Riccardo Barbano, Vincent Dutordoir, Emile Mathieu, Urszula Julia Komorowska, and Pietro Lio. DEFT: Efficient fine-tuning of diffusion models by learning the generalised \$h\$-transform. In *The Thirty-eighth Annual Conference on Neural Information Processing Systems*, 2024. URL https://openreview.net/forum?id=AKBTFQhCjm.
 - Laurent Dinh, Jascha Sohl-Dickstein, and Samy Bengio. Density Estimation Using Real NVP. In *International Conference on Learning Representations*, pp. 32, 2017.
 - Carles Domingo-Enrich, Michal Drozdzal, Brian Karrer, and Ricky T. Q. Chen. Adjoint matching: Fine-tuning flow and diffusion generative models with memoryless stochastic optimal control. In *The Thirteenth International Conference on Learning Representations*, 2025. URL https://openreview.net/forum?id=xQBRrtQM8u.
 - Esscher. On the probability function in the collective theory of risk. *Scandinavian Actuarial Journal*, 1932(3):175–195, 1932. doi: 10.1080/03461238.1932.10405883. URL https://doi.org/10.1080/03461238.1932.10405883.
 - Patrick Esser, Sumith Kulal, Andreas Blattmann, Rahim Entezari, Jonas Müller, Harry Saini, Yam Levi, Dominik Lorenz, Axel Sauer, Frederic Boesel, Dustin Podell, Tim Dockhorn, Zion English, Kyle Lacey, Alex Goodwin, Yannik Marek, and Robin Rombach. Scaling rectified flow transformers for high-resolution image synthesis, 2024. URL https://arxiv.org/abs/2403.03206.
 - Stephanie Fu, Netanel Yakir Tamir, Shobhita Sundaram, Lucy Chai, Richard Zhang, Tali Dekel, and Phillip Isola. Dreamsim: Learning new dimensions of human visual similarity using synthetic data. In *Thirty-seventh Conference on Neural Information Processing Systems*, 2023. URL https://openreview.net/forum?id=DEiNSfh1k7.

Marylou Gabrié, Grant M. Rotskoff, and Eric Vanden-Eijnden. Adaptive monte carlo augmented with normalizing flows. *Proceedings of the National Academy of Sciences*, 119(10):e2109420119, 2022. doi: 10.1073/pnas.2109420119. URL https://www.pnas.org/doi/abs/10.1073/pnas.2109420119.

- Tomas Geffner, Kieran Didi, Zuobai Zhang, Danny Reidenbach, Zhonglin Cao, Jason Yim, Mario Geiger, Christian Dallago, Emine Kucukbenli, Arash Vahdat, and Karsten Kreis. Proteina: Scaling flow-based protein structure generative models. In *International Conference on Learning Representations (ICLR)*, 2025.
- Aaron Havens, Benjamin Kurt Miller, Bing Yan, Carles Domingo-Enrich, Anuroop Sriram, Brandon Wood, Daniel Levine, Bin Hu, Brandon Amos, Brian Karrer, Xiang Fu, Guan-Horng Liu, and Ricky T. Q. Chen. Adjoint sampling: Highly scalable diffusion samplers via adjoint matching, 2025. URL https://arxiv.org/abs/2504.11713.
- Lukas Herron, Kinjal Mondal, John S. Schneekloth, and Pratyush Tiwary. Inferring phase transitions and critical exponents from limited observations with thermodynamic maps. *Proceedings of the National Academy of Sciences*, 121(52):e2321971121, 2024. doi: 10.1073/pnas.2321971121. URL https://www.pnas.org/doi/abs/10.1073/pnas.2321971121.
- Jack Hessel, Ari Holtzman, Maxwell Forbes, Ronan Le Bras, and Yejin Choi. CLIPScore: A reference-free evaluation metric for image captioning. In Marie-Francine Moens, Xuan-jing Huang, Lucia Specia, and Scott Wen-tau Yih (eds.), *Proceedings of the 2021 Conference on Empirical Methods in Natural Language Processing*, pp. 7514–7528, Online and Punta Cana, Dominican Republic, November 2021. Association for Computational Linguistics. doi: 10.18653/v1/2021.emnlp-main.595. URL https://aclanthology.org/2021.emnlp-main.595/.
- Jonathan Ho, Ajay Jain, and Pieter Abbeel. Denoising diffusion probabilistic models. In *Advances in neural information processing systems*, volume 33, pp. 6840–6851, 2020.
- Matthew D. Hoffman and Andrew Gelman. The no-u-turn sampler: Adaptively setting path lengths in hamiltonian monte carlo, 2011. URL https://arxiv.org/abs/1111.4246.
- Peter Holderrieth, Michael S. Albergo, and Tommi Jaakkola. Leaps: A discrete neural sampler via locally equivariant networks, 2025. URL https://arxiv.org/abs/2502.10843.
- Gurtej Kanwar, Michael S. Albergo, Denis Boyda, Kyle Cranmer, Daniel C. Hackett, Sébastien Racanière, Danilo Jimenez Rezende, and Phiala E. Shanahan. Equivariant flow-based sampling for lattice gauge theory. *Phys. Rev. Lett.*, 125:121601, Sep 2020. doi: 10.1103/PhysRevLett. 125.121601. URL https://link.aps.org/doi/10.1103/PhysRevLett.125.121601.
- Jonas Köhler, Leon Klein, and Frank Noe. Equivariant flows: Exact likelihood generative learning for symmetric densities. In Hal Daumé III and Aarti Singh (eds.), *Proceedings of the 37th International Conference on Machine Learning*, volume 119 of *Proceedings of Machine Learning Research*, pp. 5361–5370. PMLR, 13–18 Jul 2020. URL https://proceedings.mlr.press/v119/kohler20a.html.
- Yaron Lipman, Ricky TQ Chen, Heli Ben-Hamu, Maximilian Nickel, and Matthew Le. Flow matching for generative modeling. In *The Eleventh International Conference on Learning Representations*, 2022.
- Xingchao Liu, Chengyue Gong, and Qiang Liu. Flow straight and fast: Learning to generate and transfer data with rectified flow. In *The Eleventh International Conference on Learning Representations*, 2022.
- Zhen Liu, Tim Z. Xiao, Weiyang Liu, Yoshua Bengio, and Dinghuai Zhang. Efficient diversity-preserving diffusion alignment via gradient-informed GFlownets. In *The Thirteenth International Conference on Learning Representations*, 2025. URL https://openreview.net/forum?id=Aye5wL6TCn.

- Youssef Marzouk, Tarek Moselhy, Matthew Parno, and Alessio Spantini. Sampling via measure transport: An introduction. *Handbook of uncertainty quantification*, 1:2, 2016.
 - Bálint Máté and François Fleuret. Learning interpolations between boltzmann densities, 2023. URL https://arxiv.org/abs/2301.07388.
 - Radford M. Neal. Probabilistic inference using markov chain monte carlo methods. Technical Report CRG-TR-93-1, Department of Computer Science, University of Toronto, September 1993.
 - Kim A. Nicoli, Christopher J. Anders, Lena Funcke, Tobias Hartung, Karl Jansen, Pan Kessel, Shinichi Nakajima, and Paolo Stornati. Estimation of thermodynamic observables in lattice field theories with deep generative models. *Phys. Rev. Lett.*, 126:032001, Jan 2021. doi: 10.1103/PhysRevLett.126.032001. URL https://link.aps.org/doi/10.1103/PhysRevLett.126.032001.
 - Frank Noé, Simon Olsson, Jonas Köhler, and Hao Wu. Boltzmann generators: Sampling equilibrium states of many-body systems with deep learning. *Science*, 365(6457):eaaw1147, 2019. doi: 10.1126/science.aaw1147. URL https://www.science.org/doi/abs/10.1126/science.aaw1147.
 - Michael Plainer, Hao Wu, Leon Klein, Stephan Günnemann, and Frank Noé. Consistent sampling and simulation: Molecular dynamics with energy-based diffusion models, 2025. URL https://arxiv.org/abs/2506.17139.
 - Danilo Rezende and Shakir Mohamed. Variational Inference with Normalizing Flows. In *International Conference on Machine Learning*, pp. 1530–1538. PMLR, June 2015.
 - Robin Rombach, Andreas Blattmann, Dominik Lorenz, Patrick Esser, and Björn Ommer. High-resolution image synthesis with latent diffusion models. In *Proceedings of the IEEE/CVF conference on computer vision and pattern recognition*, pp. 10684–10695, 2022.
 - Amirmojtaba Sabour, Sanja Fidler, and Karsten Kreis. Align your flow: Scaling continuous-time flow map distillation, 2025. URL https://arxiv.org/abs/2506.14603.
 - Victor Garcia Satorras, Emiel Hoogeboom, and Max Welling. E(n) equivariant graph neural networks, 2022. URL https://arxiv.org/abs/2102.09844.
 - Yang Song, Jascha Sohl-Dickstein, Diederik P Kingma, Abhishek Kumar, Stefano Ermon, and Ben Poole. Score-based generative modeling through stochastic differential equations. arXiv:2011.13456, 2020.
 - Yifeng Tian, Nishant Panda, and Yen Ting Lin. Liouville flow importance sampler. In Ruslan Salakhutdinov, Zico Kolter, Katherine Heller, Adrian Weller, Nuria Oliver, Jonathan Scarlett, and Felix Berkenkamp (eds.), *Proceedings of the 41st International Conference on Machine Learning*, volume 235 of *Proceedings of Machine Learning Research*, pp. 48186–48210. PMLR, 21–27 Jul 2024. URL https://proceedings.mlr.press/v235/tian24c.html.
 - Belinda Tzen and Maxim Raginsky. Theoretical guarantees for sampling and inference in generative models with latent diffusions, 2019. URL https://arxiv.org/abs/1903.01608.
 - Francisco Vargas, Will Grathwohl, and Arnaud Doucet. Denoising diffusion samplers, 2023. URL https://arxiv.org/abs/2302.13834.
 - Francisco Vargas, Shreyas Padhy, Denis Blessing, and Nikolas Nüsken. Transport meets variational inference: Controlled monte carlo diffusions. In *The Twelfth International Conference on Learning Representations*, 2024. URL https://openreview.net/forum?id=PP1rudnxiW.
 - Bram Wallace, Meihua Dang, Rafael Rafailov, Linqi Zhou, Aaron Lou, Senthil Purushwalkam, Stefano Ermon, Caiming Xiong, Shafiq Joty, and Nikhil Naik. Diffusion model alignment using direct preference optimization. In *Proceedings of the IEEE/CVF Conference on Computer Vision and Pattern Recognition (CVPR)*, pp. 8228–8238, June 2024.

Joseph L. Watson, David Juergens, Nathaniel R. Bennett, Brian L. Trippe, Jason Yim, Helen E. Eisenach, Woody Ahern, Andrew J. Borst, Robert J. Ragotte, Lukas F. Milles, Basile I. M. Wicky, Nikita Hanikel, Samuel J. Pellock, Alexis Courbet, William Sheffler, Jue Wang, Preetham Venkatesh, Isaac Sappington, Susana Vázquez Torres, Anna Lauko, Valentin De Bortoli, Emile Mathieu, Sergey Ovchinnikov, Regina Barzilay, Tommi S. Jaakkola, Frank DiMaio, Minkyung Baek, and David Baker. De novo design of protein structure and function with rfdiffusion. Nature, 620(7976):1089–1100, 2023.

Xiaoshi Wu, Yiming Hao, Keqiang Sun, Yixiong Chen, Feng Zhu, Rui Zhao, and Hongsheng Li. Human preference score v2: A solid benchmark for evaluating human preferences of text-to-image synthesis, 2023. URL https://arxiv.org/abs/2306.09341.

Jiazheng Xu, Xiao Liu, Yuchen Wu, Yuxuan Tong, Qinkai Li, Ming Ding, Jie Tang, and Yuxiao Dong. Imagereward: Learning and evaluating human preferences for text-to-image generation. In A. Oh, T. Naumann, A. Globerson, K. Saenko, M. Hardt, and S. Levine (eds.), *Advances in Neural Information Processing Systems*, volume 36, pp. 15903–15935. Curran Associates, Inc., 2023. URL https://proceedings.neurips.cc/paper_files/paper/2023/file/33646ef0ed554145eab65f6250fab0c9-Paper-Conference.pdf.

Claudio Zeni, Robert Pinsler, Daniel Zügner, Andrew Fowler, Matthew Horton, Xiang Fu, Zilong Wang, Aliaksandra Shysheya, Jonathan Crabbé, Shoko Ueda, Roberto Sordillo, Lixin Sun, Jake Smith, Bichlien Nguyen, Hannes Schulz, Sarah Lewis, Chin-Wei Huang, Ziheng Lu, Yichi Zhou, Han Yang, Hongxia Hao, Jielan Li, Chunlei Yang, Wenjie Li, Ryota Tomioka, and Tian Xie. A generative model for inorganic materials design. *Nature*, 2025. doi: 10.1038/s41586-025-08628-5.

Dinghuai Zhang, Yizhe Zhang, Jiatao Gu, Ruixiang Zhang, Josh Susskind, Navdeep Jaitly, and Shuangfei Zhai. Improving gflownets for text-to-image diffusion alignment, 2024. URL https://arxiv.org/abs/2406.00633.

Qinsheng Zhang and Yongxin Chen. Path integral sampler: a stochastic control approach for sampling, 2022. URL https://arxiv.org/abs/2111.15141.

A Proofs

 Proposition 1. (Covariance ODE.) Let $I_t^a = \alpha_t x_0 + \beta_t x_1^a$ be the interpolant constructed from samples $x_1^a \sim \rho_{1,a}(x)$. Then the augmented drift $b_{t,a}(x)$ satisfies

$$\frac{\partial b_{t,a}(x)}{\partial a} = \mathbb{E}[\dot{I}_t^a r(x_1^a) | I_t^a = x] - b_{t,a}(x) \, \mathbb{E}[r(x_1^a) | I_t^a = x], \qquad b_{t,a=0}(x) = b_t(x) \tag{8}$$

where the expectation is taken over the law of I_t^a conditional on $I_t^a = x$. The right-hand side of this equation is the conditional covariance $\operatorname{Cov}_a(\dot{I}_t^a, r(x_1^a) | I_t^a = x)$.

Proof. To show equation 8, note that the pdf of I_t^a is given explicitly as

$$\rho_{t,a}(x) = \mathbb{E}[\delta(x - I_t^0)e^{ar(x_1^0)}],\tag{26}$$

where $x_0 \sim \rho_0, x_1^0 \sim \rho_{1,0}$ and we ignore the normalizing constant as it will not be relevant for the proof. Taking the time derivative on both sides of this equation

$$-\nabla \cdot (b_{t,a}(x)\rho_{t,a}(x)) = -\nabla \cdot \mathbb{E}[\dot{I}_t^0 \delta(x - I_t^0) e^{ar(x_1^0)}]$$
(27)

where we assume $\rho_{t,a}(x) > 0$ else $b_{t,a}(x) = 0$. Isolating $b_{t,a}(x)$ gives

$$b_{t,a}(x) = \frac{\mathbb{E}[\dot{I}_t^0 \delta(x - I_t^0) e^{ar(x_1^0)}]}{\mathbb{E}[\delta(x - I_t^0) e^{ar(x_1^0)}]}.$$
 (28)

Dividing the numerator and denominator by $\mathbb{E}[\delta(x-I_t^0)]$ proves equation 6. Taking its derivative with respect to a and using the quotient rule, we have

$$\frac{\partial}{\partial a}b_{t,a}(x) = \frac{\mathbb{E}[\dot{I}_{t}^{0}\delta(x-I_{t}^{0})e^{ar(x_{1}^{0})}r(x_{1}^{0})]}{\mathbb{E}[\delta(x-I_{t}^{0})e^{ar(x_{1}^{0})}]} - \frac{\mathbb{E}[\dot{I}_{t}^{0}\delta(x-I_{t}^{0})e^{ar(x_{1}^{0})}]}{\mathbb{E}[\delta(x-I_{t}^{0})e^{ar(x_{1}^{0})}]} \frac{\mathbb{E}[\delta(x-I_{t}^{0})e^{ar(x_{1}^{0})}]}{\mathbb{E}[\delta(x-I_{t}^{0})e^{ar(x_{1}^{0})}]}$$
(29)

$$= \mathbb{E}[\dot{I}_t^a r(x_1^a) | I_t^a = x] - b_{t,a}(x) \, \mathbb{E}[r(x_1^a) | I_t^a = x], \tag{30}$$

which completes the proof.

Proposition 2. (Explicit Tilt Matching.) Assume $a \mapsto b_{t,a}(x)$ is C^1 with $\partial_a b_{t,a}$ given by (8), and let h > 0. Then, the unique minimizer of the regression objective

$$\mathcal{L}_{a\to a+h}^{\text{ETM}}(\hat{b}) := \int_{0}^{1} \mathbb{E} \left\| \hat{b}_{t}(I_{t}^{a}) - T_{t,a,h} \right\|^{2} dt.$$
 (12)

is given by

$$\hat{b}_{t,a+h}(x) = \mathbb{E}^a[T_{t,a,h} \mid I_t^a = x]. \tag{13}$$

As such, training $\hat{b}_{t,a+h}$ to optimality on (12) produces a first-order accurate Euler update of the tilted velocity. Iterating for $a_k = kh$ with samples $x_1^{a_k}$ drawn using the current model defines a consistent scheme that converges to $b_{t,1}$ as $h \to 0$ under the above regularity.

Proof. By the Hilbert L^2 projection theorem, among all functions of I_t^a , the optimizer is the condtional expectation $\mathbb{E}^a[T_{t,a,h} \mid I_t^a = x]$ where again \mathbb{E}^a denotes expectation over the coupling (x_0, x_1^a) . Expanding $b_{t,a+h} = b_{t,a} + h \, \partial_a b_{t,a} + \mathcal{O}(h^2)$ and using (8) yields the expression above. \square

Proposition 3. (Tilt expansion.) For $b_{t,a} = \mathbb{E}[\dot{I}_t^a | I_t^a = x]$, the n^{th} term $\frac{\partial^n}{\partial a^n}[b_{t,a}(x)]$ in the expansion in (14) is the $(n+1)^{th}$ order joint cumulant of the interpolant and n instances of the reward, $\kappa^n(\dot{I}_t^a, r(x_1^a), \dots, r(x_1^a))$.

Proof. For a fixed x, define the joint conditional cumulant generating function of $r(x_1^a)$ and \dot{I}_t^a as

$$M(\mu, \nu) = \log \mathbb{E}\left[e^{\mu r(x_1^a) + \langle \nu, \dot{I}_t^a \rangle} | I_t^a = x\right],\tag{31}$$

for $\mu \in \mathbb{R}$ and $\nu \in \mathbb{R}^d$. Its partial derivative with respect to ν evaluated at 0 is

$$\frac{\partial}{\partial \nu} M(\mu, 0) = \frac{\mathbb{E}[\dot{I}_t^a e^{\mu r(x_1^a)} | I_t^a = x]}{\mathbb{E}[e^{\mu r(x_1^a)} | I_t^a = x]} = b_{t, a + \mu}(x), \tag{32}$$

where the second equality is (7). Taking n derivatives with respect to μ and evaluating at 0, we obtain

$$\frac{\partial^{n+1}}{\partial \mu^n \partial \nu} M(0,0) = \frac{\partial^n}{\partial \mu^n} b_{t,a+\mu}(x) \Big|_{\mu=0} = \frac{\partial^n}{\partial a^n} b_{t,a}(x). \tag{33}$$

The leftmost term is precisely the $(n+1)^{th}$ order joint cumulant.

Proposition 5. (Variance control). Let $\mathcal{L}_{a\to a+h}^{\mathrm{WFM}}$ and $\mathcal{L}_{a\to a+h}^{\mathrm{ITM}}$ be the regression losses in (22) and (12). For sufficiently small h, the gradient estimator of WFM has variance at least as large as that of ACM:

$$\operatorname{Var}\left[\nabla \mathcal{L}_{a \to a + h}^{\operatorname{WFM}}\right] \geq \operatorname{Var}\left[\nabla \mathcal{L}_{a \to a + h}^{\operatorname{ITM}}\right].$$
 (23)

Proof. The first variation (the Gateaux derivative) of the loss $\mathcal{L}_{a \to a+h}^{c-\mathrm{ITM}}$ is

$$\delta \mathcal{L}_{a \to a + h}^{\text{c-ITM}}(\hat{b}) = 2 \int_{0}^{1} \mathbb{E}\left[c(I_{t}^{a})\left(\hat{b}_{t}(I_{t}^{a}) - b_{t,a}(I_{t}^{a})\right) + \left(e^{hr(x_{1}^{a})} - c(I_{t}^{a})\right)\left(\hat{b}_{t}(I_{t}^{a}) - \dot{I}_{t}^{a}\right)\right] dt. \quad (34)$$

Therefore the Monte Carlo estimator used is

$$\xi_c := 2 \Big(c(I_t^a) \left(\hat{b}_t(I_t^a) - b_{t,a}(I_t^a) \right) + \left(e^{hr(x_1^a)} - c(I_t^a) \right) \left(\hat{b}_t(I_t^a) - \dot{I}_t^a \right) \Big)$$
(35)

where $t \sim \text{Unif}[0, 1]$. We will use the law of total variance

$$Var(\xi_c) = \mathbb{E}[Var(\xi_c|I_t^a)] + Var(\mathbb{E}[\xi_c|I_t^a]). \tag{36}$$

Notice that

$$\mathbb{E}[\xi_c|I_t^a] = \mathbb{E}\left[e^{hr(x_1^a)}(\hat{b}_t(I_t^a) - \dot{I}_t^a)|I_t^a\right]$$
(37)

is independent of c and therefore the same for any c-ITM variant. On the other hand, we have that

$$Var(\xi_c|I_t^a) = Var\left(e^{hr(x_1^a)}(\hat{b}_t(I_t^a) - \dot{I}_t^a) + c(I_t^a)\dot{I}_t^a|I_t^a\right).$$
(38)

Writing $e^{hr(x_1^a)} = 1 + \mathcal{O}(h)$, we see that

$$\mathbb{E}\left[\operatorname{Var}(\xi_c|I_t^a)\right] = \mathbb{E}\left[\operatorname{Var}\left((1 - c(I_t^a))\dot{I}_t^a|I_t^a\right)\right] + \mathcal{O}(h). \tag{39}$$

Recall that $\mathcal{L}^{\mathrm{ITM}}_{a \to a + h}$ corresponds to taking c(x) = 1 and $\mathcal{L}^{\mathrm{WFM}}_{a \to a + h}$ is c(x) = 0. When c(x) = 1, we have $\mathbb{E}\left[\mathrm{Var}(\xi_c|I^a_t)] = \mathcal{O}(h)$. When c(x) = 0, we have $\mathbb{E}\left[\mathrm{Var}(\xi_c|I^a_t)] = \mathbb{E}[\mathrm{Var}(\dot{I}^a_t|I^a_t)] + \mathcal{O}(h)$. Provided that $\mathbb{E}[\mathrm{Var}(\dot{I}^a_t|I^a_t)] > 0$, this completes the proof. We remark that $\mathbb{E}[\mathrm{Var}(\dot{I}^a_t|I^a_t)] = 0$ occurs only for a very limited collection of couplings $\rho(x_0, x_1^a)$, such as the optimal transport coupling and would not be feasible in practice. Note that when \hat{b} takes a parametric form, a similar proof holds.

B EXPERIMENTS

B.1 Sampling Lennard-Jones Potentials

The Lennard-Jones (LJ) potential is a widely used mathematical model that describes the potential energy between two neutral, non-bonding particles. This energy is calculated as a function of the distances between particles, capturing the balance between long-range attractive forces and short-range repulsive forces. It has the form

$$E^{LJ}(x) = \frac{\epsilon}{2\tau} \sum_{ij} \left(\left(\frac{r_m}{d_{ij}} \right)^6 - \left(\frac{r_m}{d_{ij}} \right)^{12} \right), \tag{40}$$

where $d_{ij} = \|x_i - x_j\|$ is the distance between particles i and j, ϵ is the potential well depth, r_m is the equilibrium distance at which the potential is minimized, and τ is the system temperature. We follow Köhler et al. (2020); Akhound-Sadegh et al. (2025) in adding a harmonic potential to the energy:

$$E^{\text{Total}}(x) = E^{\text{LJ}}(x) + \frac{1}{2} \sum_{i} ||x_i - \bar{x}||^2, \tag{41}$$

where \bar{x} is the center of mass of the system. We use the same parameters $\epsilon=2.0, r_m=1$ and $\tau=1$ as Akhound-Sadegh et al. (2025) for our experiments. For the LJ-13 and LJ-55 datasets we use samples provided by the codebase in Akhound-Sadegh et al. (2025) which use the No-U-Turn-Sampler (NUTS) Hoffman & Gelman (2011).

In our experiments we use an EGNN Satorras et al. (2022). For LJ-13 we use three layers and 32 hidden dimensions which is approximately 45,000 parameters. For LJ-55 we use five layers and 128 hidden dimensions for a parameter count of approximately 580,000.

To compute the Effective Sample Size (ESS) we evaluate likelihoods $p_1(x_1)$ under our model b_t by

$$\log p_1(x_1) = \log p_0(x_0) - \int_0^1 \nabla \cdot \hat{b}_t(x_t) dt$$
 (42)

to compute importance weights $w(x_1) = \frac{\rho_{1,a=0}(x_1)e^{r(x_1)}}{p_1(x_1)}$ and then compute the ESS as

$$ESS = \frac{\left(\sum_{i=1}^{N} w_i\right)^2}{N \sum_{i=1}^{N} w_i^2}.$$
 (43)

```
810
            Algorithm 1: Tilt Matching (TM)
811
            Input: Pretrained drift b_{t,0}; reward r(x); annealing schedule \{a_k\}_{k=0}^K with steps h_k = a_{k+1} - a_k;
812
                      interpolant I_t^a (linear shown); epochs E; batch size B, ETM or ITM.
813
            Output: Tilted drift b_{t,1}.
814
            for k = 0, \dots, K-1 do
815
                 // Current model is b_{t,a_k}; goal is b_{t,a_{k+1}}
816
                 Initialize \hat{b}_t \leftarrow b_{t,a_k}
                 for epoch = 1, \dots, E do
817
                       Draw B samples (x_0, x_1^{a_k}) with x_1^{a_k} \sim \rho_{1,a_k} (from model or buffer), t \sim \text{Unif}[0,1].
818
                       I_t^{a_k} \leftarrow (1-t)x_0 + tx_1^{a_k}; \quad \dot{I}_t^{a_k} \to x_1^{a_k} - x_0
819
820
                         T_{t,a_k,h_k} \leftarrow b_{t,a_k}(I_t^{a_k}) + h_k(\dot{I}_t^{a_k}r(x_1^{a_k}) - b_{t,a}(I_t^{a_k}))r(x_1^{a_k}) 
821
                      if ITM then
822
                         [T_{t,a_k,h_k} \leftarrow b_{t,a_k}(I_t^{a_k}) + (e^{h_k r(x_1^{a_k})} - 1) (\hat{b}_t(I_t^{a_k}) - \dot{I}_t^{a_k}) ] 
823
                       \mathcal{L} \leftarrow \frac{1}{B} \sum_{t=0}^{B} \|\hat{b}_{t}(I_{t}^{a_{k}}) - T_{t,a_{k},h_{k}}\|^{2}
824
825
                     Update the parameters of \hat{b}_t by gradient descent to minimize the ITM loss
826
                 Set b_{t,a_{k+1}} \leftarrow \hat{b}_t.
                 // (Optional): a few flow-matching steps on I_t^{a_{k+1}} to recenter
828
            return b_{t,1}.
829
```

C EXAMPLE IMAGES FROM FINE-TUNING EXPERIMENTS

In this appendix, we display a random selection of images from the base model and the model fine-tuned under the Euler Tilt Matching objective. It can be seen that images generated from the fine-tuned model better adhere to the given text prompt, which aligns with the numerical results in the main text.











Figure 5: Images generated from the base model with prompt: *old man (long white beard and a hood) riding on lions back*











Figure 6: Images generated from the Tilt Matching fine-tuned model with prompt: old man (long white beard and a hood) riding on lions back











Figure 7: Images generated from the base model with prompt: *astronaut drifting afloat in space, in the darkness away from anyone else, alone, black background dotted with stars, realistic*









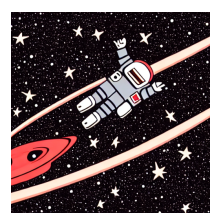


Figure 8: Images generated from the Tilt Matching fine-tuned model with prompt: astronaut drifting afloat in space, in the darkness away from anyone else, alone, black background dotted with stars, realistic

LLM USAGE

In preparing this paper, we used large language models (LLMs) as assistive tools. Specifically, LLMs were used for (i) editing and polishing the text for clarity and readability, and (ii) formatting matplotlib code. The authors take full responsibility for the content of this paper.